Cell Reports

Report

The apparent loss of PRC2 chromatin occupancy as an artifact of RNA depletion

Graphical abstract

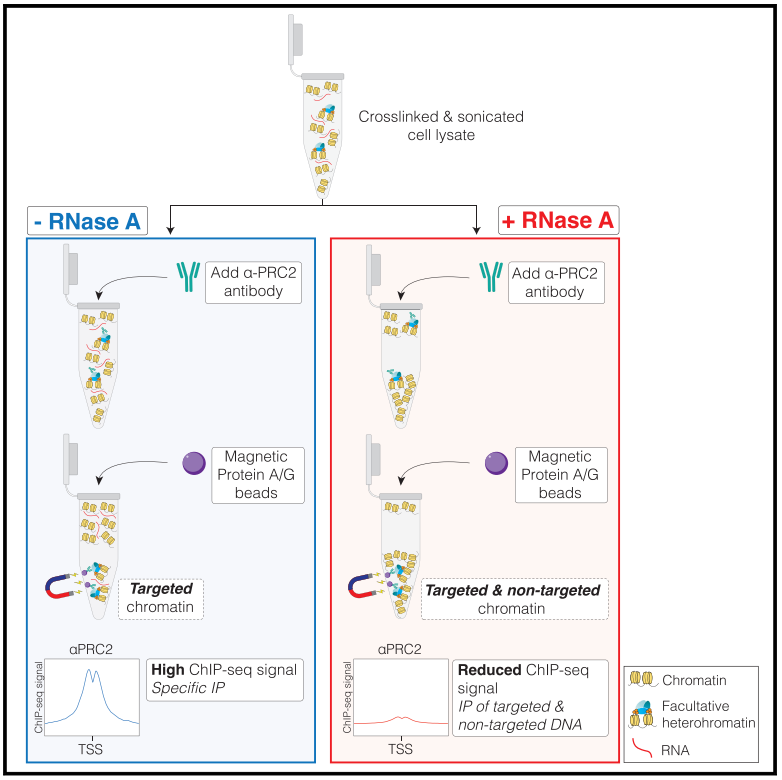

Highlights

- RNA degradation during ChIP-seq is insufficient to displace PRC2 from chromatin
- RNA degradation leads to the artificial depletion of ChIP-seq signals in multiple cell lines
- Artificially reduced ChIP-seq signals are explained by a gain of non-targeted DNA
- RNA is critical in maintaining the solubility of chromatin during experimentation

Authors

Evan Healy, Qi Zhang, Emma H. Gail, ..., Partha Pratim Das, Jose M. Polo, Chen Davidovich

Correspondence

chen.davidovich@monash.edu

In brief

Healy et al. demonstrate that RNase A treatment of chromatin during immunoprecipitation leads to the artificial loss of all facultative heterochromatin. This observation can be explained by a gain in non-targeted chromatin that is sequenced at the expense of DNA from facultative heterochromatin, which reduces ChIP signals.

Healy et al., 2024, Cell Reports *43*, 113858
March 26, 2024
https://doi.org/10.1016/j.celrep.2024.113858

CellPress

Cell Reports

CellPress
OPEN ACCESS

Report

The apparent loss of PRC2 chromatin occupancy as an artifact of RNA depletion

Evan Healy,[1,8] Qi Zhang,[1,2,3,8] Emma H. Gail,[1] Samuel C. Agius,[1] Guizhi Sun,[4] Michael Bullen,[5] Varun Pandey,[5] Partha Pratim Das,[4,5] Jose M. Polo,[4,5,6] and Chen Davidovich[1,7,9,*]

[1]Department of Biochemistry and Molecular Biology, Biomedicine Discovery Institute, Faculty of Medicine, Nursing and Health Sciences, Monash University, Clayton, VIC, Australia
[2]South Australian immunoGENomics Cancer Institute (SAiGENCI), Faculty of Health and Medical Sciences, University of Adelaide, Adelaide, SA, Australia
[3]EMBL-Australia at SAiGENCI, Adelaide, SA, Australia
[4]Development and Stem Cells Program, Monash Biomedicine Discovery Institute, Wellington Road, Clayton, VIC 3800, Australia
[5]Department of Anatomy and Developmental Biology, Monash University, Wellington Road, Clayton, VIC 3800, Australia
[6]Adelaide Centre for Epigenetics and South Australian immunoGENomics Cancer Institute, Faculty of Health and Medical Sciences, The University of Adelaide, Adelaide, SA, Australia
[7]EMBL-Australia, Clayton, VIC, Australia
[8]These authors contributed equally
[9]Lead contact
*Correspondence: chen.davidovich@monash.edu
https://doi.org/10.1016/j.celrep.2024.113858

SUMMARY

RNA has been implicated in the recruitment of chromatin modifiers, and previous studies have provided evidence in favor and against this idea. RNase treatment of chromatin is commonly used to study RNA-mediated regulation of chromatin modifiers, but the limitations of this approach remain unclear. RNase A treatment during chromatin immunoprecipitation (ChIP) reduces chromatin occupancy of the H3K27me3 methyltransferase Polycomb repressive complex 2 (PRC2). This led to suggestions of an "RNA bridge" between PRC2 and chromatin. Here, we show that RNase A treatment during ChIP causes the apparent loss of all facultative heterochromatin, including both PRC2 and H3K27me3 genome-wide. We track this observation to a gain of DNA from non-targeted chromatin, sequenced at the expense of DNA from facultative heterochromatin, which reduces ChIP signals. Our results emphasize substantial limitations in using RNase A treatment for mapping RNA-dependent chromatin occupancy and invalidate conclusions that were previously established for PRC2 based on this assay.

INTRODUCTION

Much of the mammalian genome is transcribed,[1] with many of these RNAs being retained in the nucleus. RNA that is localized to chromatin can have crucial roles in gene expression and chromatin regulation.[2–7] RNA has been proposed to serve an architectural role in chromatin organization, with its depletion leading to disruption of both active and repressed chromatin domains.[8–11] Many chromatin modifiers physically interact with RNA, and direct roles of RNA in their recruitment to target genes have been proposed.[12] Among the most studied chromatin modifiers in the context of RNA-mediated recruitment is the H3K27me3 methyltransferase Polycomb repressive complex 2 (PRC2).

The enzymatic activity and localization of PRC2 are critical for the repression of cell-type-specific genes during embryonic development and are often perturbed in disease.[13–15] PRC2 interacts with RNA promiscuously,[16] explained by preferences for prevalent G-tract sequences.[17,18] A functional role of PRC2-RNA interactions has been intensely debated, with seemingly opposing models proposed, such as RNA-mediated recruitment of PRC2 or antagonistic interactions (reviewed in Almeida et al.[19] and Davidovich and Cech[19,20]). Further studies have explained aspects of PRC2 recruitment that may occur without RNA involvement.[21–24] At present, there is ambiguity on how—and to what extent—RNA regulates the chromatin occupancy of PRC2 despite increased usage of perturbation experiments.[18,25–27]

For the past few decades, a common perturbation experiment for the study of RNA-mediated regulation of chromatin has been through RNase treatment.[6,9,25,28–35] More recently, RNase treatment of chromatin has been used to ascribe functional roles of RNA in the regulation of PRC2 and facultative heterochromatin.[11,25,26] When nuclei are treated with RNase A, chromatin immunoprecipitation sequencing (ChIP-seq) indicates a gain of PRC2 on chromatin.[25] These data were used to support a model where RNA antagonizes PRC2 chromatin binding to dictate the genome-wide localization patterns of PRC2. Conversely, when chromatin was first isolated from cells and subsequently treated with RNase A, ChIP-seq indicated the depletion of PRC2 subunits from chromatin.[26] Data that were generated using this method were used to support a model where RNA is required

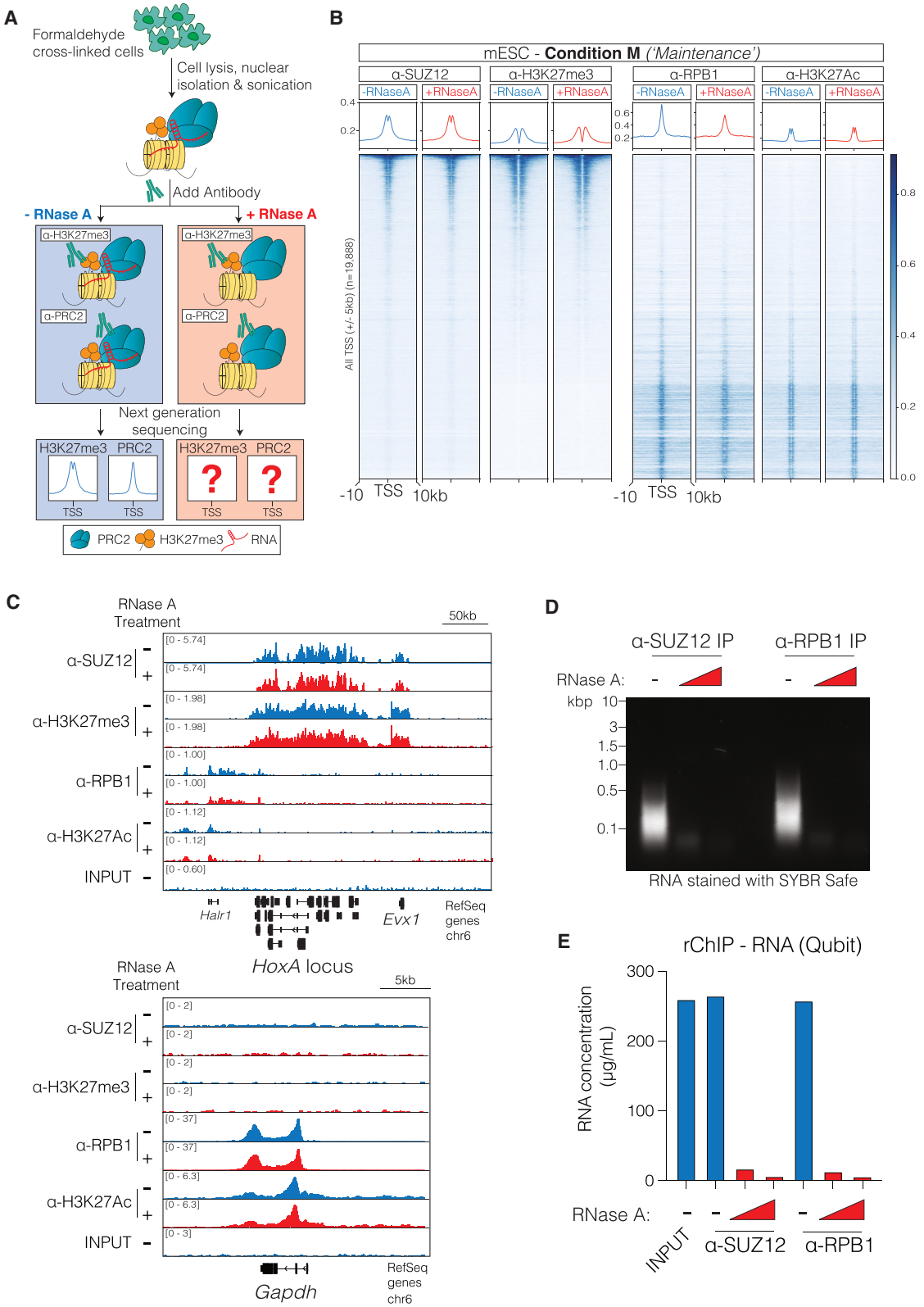

(legend on next page)

for PRC2 chromatin occupancy through an "RNA bridge."[26] These seemingly contradictory observations emphasize a potential problem with the interpretation of ChIP-seq results if carried out with RNase treatment. The treatment of chromatin with RNAse A during ChIP, previously termed either rChIP[26] or RNase-ChIP,[35] is referred to here as rChIP. While the usage of RNase treatment of chromatin is on the rise, its effect on the properties of chromatin during immunoprecipitation remains unclear.

Here we show that rChIP reduces the apparent PRC2 chromatin occupancy, consistent with previous observations.[26] However, the reduction in PRC2 ChIP signal is accompanied by a decrease in H3K27me3 ChIP signal genome wide. We track this observation to a global gain of non-targeted chromatin, which takes place during immunoprecipitation if performed with RNase A treatment. As a result, RNase A treatment leads to excess DNA from non-targeted genomic regions. That non-targeted DNA is then sequenced at the expense of DNA from facultative heterochromatin, resulting in the artificial loss of ChIP signals. Collectively, our results point to substantial technical limitations with the usage of rChIP and its application to PRC2. Our results also imply broader limitations of rChIP to other facultative heterochromatin regulators and possibly beyond.

RESULTS

The depletion of RNA during ChIP is insufficient to change the chromatin occupancy of PRC2

To profile genome-wide PRC2 chromatin occupancy in the context of RNA depletion, we performed ChIP-seq in the presence and absence of RNase A (rChIP) in mouse embryonic stem cells (mESCs). The ChIP-seq conditions used in this assay have been successfully applied in many previous studies[21,36–41] and are referred to here as "condition M" (where "M" stands for "maintenance"; see assay conditions in Table S1 and STAR Methods). This ChIP protocol was modified to include the addition of RNase A (i.e., rChIP) to the assay after crosslinking and during the immunoprecipitation step, as described previously[26] (Figure 1A). Under these rChIP conditions (Table S1), RNase A treatment did not affect PRC2 chromatin occupancy (Figures 1B and 1C). We extended this analysis to RPB1, an RNA polymerase II (RNA Pol II) subunit associated with active chromatin, and again observed no substantial RNase-dependent changes to its chromatin occupancy (Figures 1B and 1C). We next confirmed that RNase A effectively eliminates RNA under these ChIP conditions (condition M; Figures 1D and 1E). Accordingly, we were also able to detect SUZ12, EZH2, and H3K27me3 enrichment at PRC2 target genes via ChIP-qPCR, either in the presence or absence of RNase A treatment (Figures S1A–S1C). These results indicate that RNA is dispensable for the retention of PRC2 on chromatin under experimental conditions that enable quality detection of ChIP-seq signals.

Loss of PRC2 occupancy following RNA depletion is accompanied by loss of H3K27me3

As we did not observe RNase A-dependent depletion of PRC2 under condition M (Figure 1), we set out to reproduce the same rChIP conditions that were used previously to identify this phenomenon[26] (Table S1; "condition L," where "L" stands for "loss"). Indeed, these ChIP conditions led to an overall reduction in chromatin-bound PRC2 (EZH2) upon RNase A treatment (Figures 2A, 2B, and S2A), as reported previously.[26] This result is seemingly in agreement with the proposed "RNA bridging" model for PRC2 chromatin binding.[26]

To further challenge the rChIP assay under condition L, we next probed for H3K27me3 as a control (Figures 2A and 2B). H3K27me3 was selected as a negative control because we had no reason to assume that an RNA bridge would be present between H3K27me3 and chromatin. Yet, the RNA-dependent reduction in PRC2 was accompanied by a concurrent loss in H3K27me3 rChIP-seq signal (Figures 2A, 2B, and S2A). This apparent loss of facultative heterochromatin following RNA depletion is consistent with another previous study that observed decreases in H3K27me3, H3K9me3, as well as CTCF upon RNase A treatment in a CUT&RUN assay.[11] Hence, the results thus far suggest that RNase treatment under condition L leads to the apparent loss of ChIP-seq signals from facultative heterochromatin, whether probing for PRC2 (α-EZH2) or repressive chromatin itself (α-H3K27me3).

RNA depletion leads to the apparent loss of H3K27me3 rChIP signals in human induced pluripotent stem cells (iPSCs) and cancer cells

All data presented to this point were generated in mESCs. Yet, previously reported rChIP experiments using antibodies for PRC2 subunits were carried out in human iPSCs.[26] Therefore, before testing the hypothesis of an rChIP-associated artifact, we first wished to determine whether the previously published rChIP conditions (condition L from Long et al.[26]) lead to the apparent depletion of H3K27me3 in human iPSCs. We therefore performed the rChIP assay in iPSCs as published previously for human iPSCs (condition L;[26] Figure 3).

Figure 1. The depletion of RNA during ChIP is insufficient to change the chromatin occupancy of PRC2

(A) Schematic illustrating the RNase-ChIP/rChIP assay (see Long et al.[26,42] and Table S1 for details on differences in ChIP conditions between figures).

(B) Heatmap representation and average enrichment profile of SUZ12, H3K27me3, RPB1, H3K27Ac, and ChIP-seq signal at all protein-coding TSSs in the presence and absence of RNase A in mESCs. Data from one representative replicate are shown. ChIP-qPCR from two further independent biological replicates are shown in Figure S1.

(C) Genome browser representation of ChIP-seq reads for SUZ12, H3K27me3, RPB1, H3K27Ac, and input following RNase A treatment at the *HOXA* gene cluster (repressed) and *GAPDH* gene locus (active).

(D) RNA was isolated following RNase A treatment (5 μg/mL or 50 μg/mL) and overnight IP with either SUZ12 or RPB1 antibodies, stained with SYBR Safe and run on an agarose gel, confirming that RNase A efficiently removes all RNA under this assay conditions.

(E) RNA was isolated following RNase A treatment (5 μg/mL or 50 μg/mL) and overnight IP with either SUZ12 or RPB1 antibodies, and RNA concentration was measured on a Qubit RNA High Sensitivity Assay Kit (Thermo Fisher Scientific, Q10211).

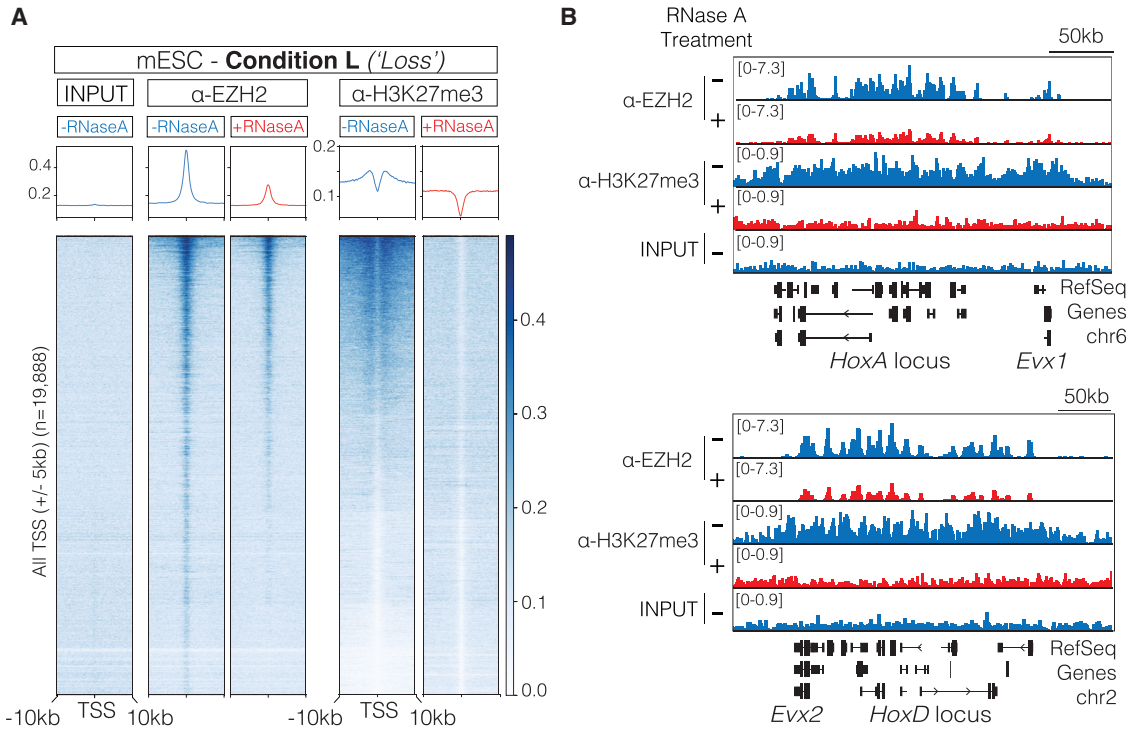

Figure 2. Experimental conditions that favor RNase-dependent depletion of PRC2 chromatin occupancy lead to a concurrent reduction of H3K27me3 ChIP signals

(A) Heatmap representation and average enrichment profile of EZH2 and H3K27me3 ChIP-seq signal at all protein-coding TSSs in the presence and absence of RNase A in mouse embryonic stem cells. One replicate is shown here, and another independent biological replicate is shown in Figure S2.

(B) Genome browser representation of ChIP-seq reads for EZH2 and H3K27me3 following RNase A treatment at both the *HOXA* and *HOXD* gene clusters.

Once more we observed a reduction in the H3K27me3 signal upon RNase A treatment (Figures 3A, 3B, S3A, and S3B), in agreement with our results using mESCs (Figure 2). We also observed this phenomenon in lineage-committed human cancer cells (K562) (Figures 3C and S3C). This suggested that RNA depletion is leading to a global loss of rChIP signals from facultative heterochromatin. As expected, the loss of H3K27me3 with RNase A treatment in iPSCs was accompanied by a loss of PRC2 (SUZ12 and EZH2; Figures S3D and S3E). Furthermore, we also saw a decrease in RPB1 and H3K27Ac rChIP-seq signals in iPSCs (Figures 3A, 3B, S3A, and S3B), suggesting that an artificial reduction of ChIP-seq signals also occurred in euchromatin. The observations thus far indicate that ChIP signals of both chromatin-bound factors and histone marks can be disrupted by RNA depletion.

RNA depletion during ChIP leads to a global gain of non-targeted DNA

The data thus far indicate that RNase treatment during ChIP under condition L (Table S1) leads to the loss of ChIP signals from facultative heterochromatin and possibly euchromatin (Figures 2 and 3). Yet, there is no obvious biological explanation for the loss of H3K27me3 after RNA depletion, as RNase treatment was carried out after chromatin was crosslinked and isolated from cells, and, hence, cannot be due to the loss of PRC2 methyltransferase activity. Therefore, we were next determined to test the hypothesis of an experimental artifact. To this end, we performed ChIP-qPCR for H3K27me3, H3K27Ac, and SUZ12 in the presence and absence of RNase A in human iPSCs under condition L. ChIP-qPCR was selected for this analysis given its ability to directly quantify the immunoprecipitation (IP) sample with respect to the input without reliance on genome-wide normalization effects.

As expected, in the absence of RNase A treatment, ChIP-qPCR identified H3K27me3 and SUZ12 at a repressed gene (*HOXA10*) and H3K27Ac on active genes (*GAPDH* and *CCNA2*; Figures 4A and S4A, blue bars). But, strikingly, RNase A treatment led to an increment of the ChIP-qPCR signal at all loci for all antibodies tested (Figures 4A and S4A, red bars). This was inconsistent with the ChIP-seq results we obtained with RNase A treatment, which reported the loss of ChIP-seq signal under the same conditions (condition L; Figures 2 and 3).

Hence, results so far are seemingly contradictory; RNase A treatment under condition L leads to a gain of ChIP-qPCR signal (Figure 4) but a loss of ChIP-seq signal (Figures 2 and 3). The simplest explanation that consolidates all of these observations is a global gain of non-targeted DNA. This is emphasized by the observation that RNase A treatment led to the unexpected gain of H3K27me3 ChIP-qPCR signal at active genes as well as the unexpected gain of H3K27Ac signals at repressed genes (Figures 4A and S4A). To directly test for an

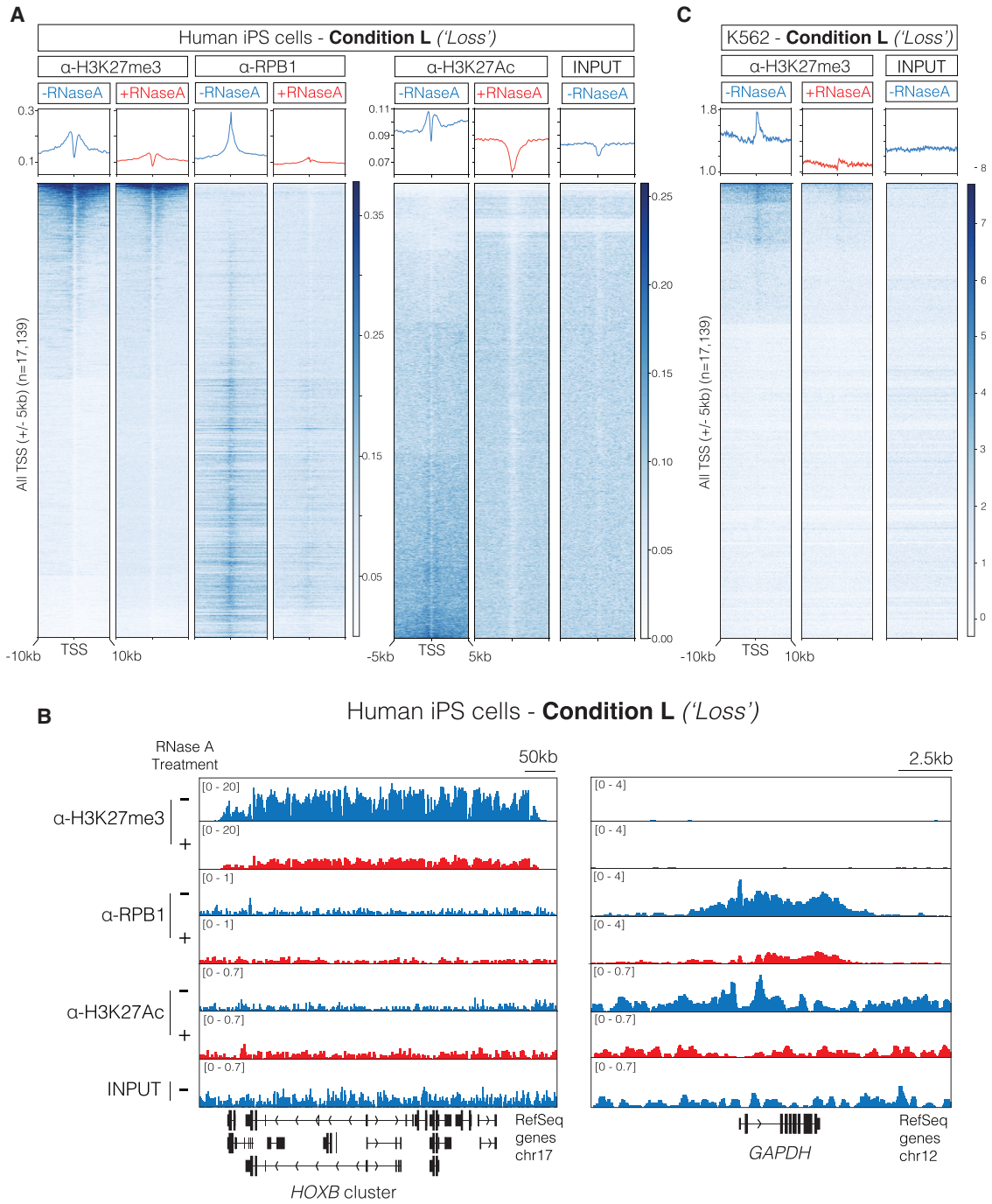

Figure 3. RNA depletion leads to the apparent loss of ChIP signals from facultative heterochromatin in human iPSCs and cancer cells

(A) Heatmap representation and average enrichment profiles of H3K27me3, RPB1, H3K27Ac, and input ChIP-seq signal at all human protein-coding TSSs in the presence and absence of RNase A in human induced pluripotent stem cells (iPSCs). Data illustrate a loss of both facultative heterochromatin (H3K27me3) and euchromatin (RPB1 and H3K27Ac) following RNA depletion. One replicate is shown here, and another independent biological replicate is shown in Figure S3.

(B) Genome browser representation of ChIP-seq reads for H3K27me3, RPB1, H3K27Ac, and input following RNase A treatment at the *HOXB* gene cluster (repressed) and *GAPDH* gene locus (active) in human iPSCs.

(C) Heatmap representation and average enrichment profile of H3K27me3 and input ChIP-seq signal at all human protein-coding TSSs in the presence and absence of RNase A in K562 human cancer cells. Experiments in this figure were carried out under condition L (see Table S1 for details on differences in ChIP conditions between figures). Data from one replicate are shown.

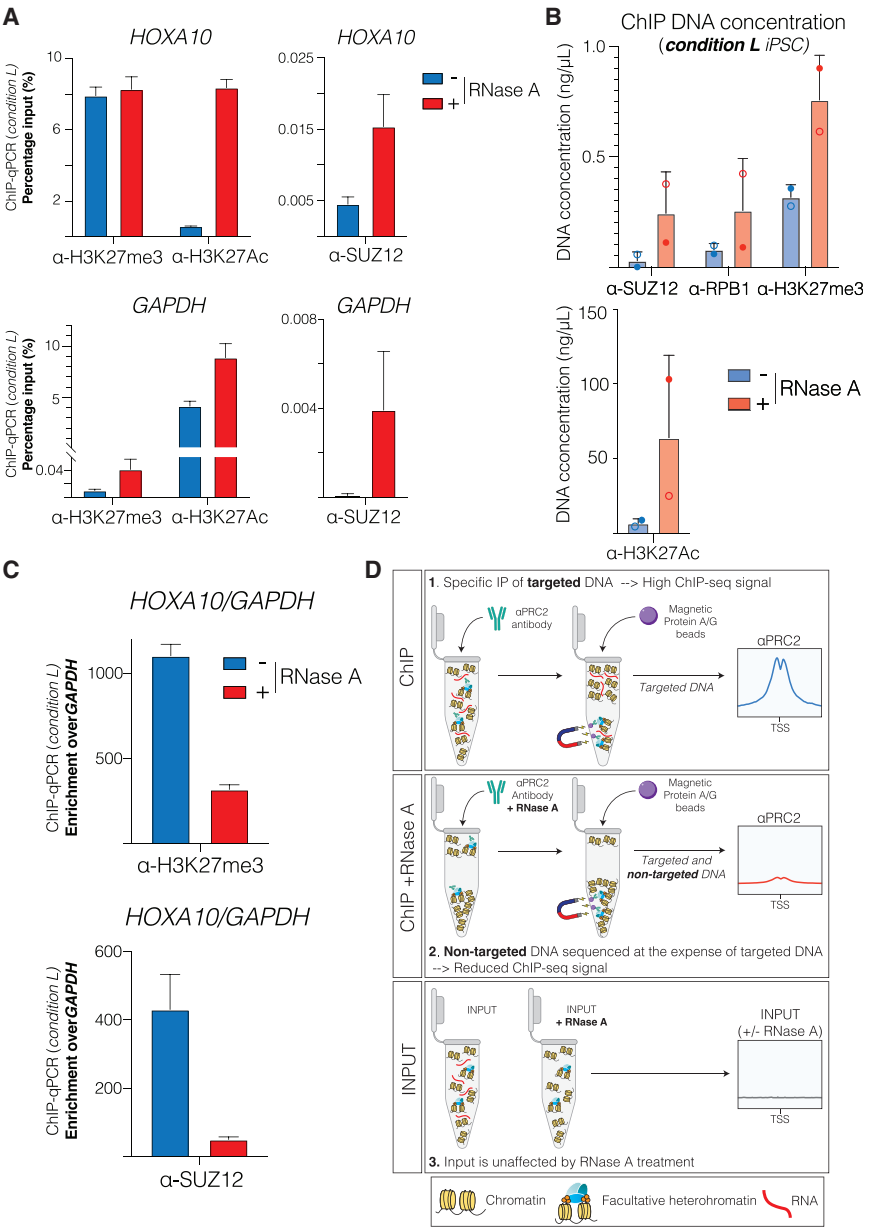

Figure 4. RNA depletion during ChIP leads to a global gain of non-targeted chromatin, which artificially reduces ChIP signals upon data normalization

(A) ChIP-qPCR analyses of H3K27me3, H3K27Ac, and SUZ12 at a representative repressed PRC2 target TSS (*HOXA10*, repressed gene) and active TSS (*GAPDH*, active gene) following RNase A treatment in human iPSCs. Enrichment is presented as a percentage of input DNA. One replicate is shown here, and an independent biological replicate is shown in Figures S4C and S4D. Error bars indicate standard deviation of qPCR triplicates.

(B) The concentration of DNA immunoprecipitated with the antibodies shown was measured on a Qubit dsDNA High Sensitivity Assay Kit (Thermo Fisher Scientific, Q32854). Qubit readings from two independent rChIP replicates are shown (solid circles, replicate 1; empty circles, replicate 2).

(C) ChIP-qPCR analyses from (A), presented as enrichment at the repressed *HOXA10* TSS normalized to a negative control TSS *GAPDH*. Error bars indicate standard deviation of qPCR triplicates.

(D) Schematic of the potential mechanism behind the loss of facultative heterochromatin after RNase A treatment in a ChIP assay. The depletion of RNA during IP reduces the solubility properties of chromatin, leading to the accumulation of both targeted and non-targeted chromatin aggregates in the IP sample. After ChIP and data normalization, the DNA from untargeted chromatin artificially reduces the signals from facultative heterochromatin. The experiments were carried out under condition L (see Table S1 for details on differences in ChIP conditions between figures).

RNase A-dependent gain of DNA, we quantified the amount of total DNA that was obtained after ChIP in the presence and absence of RNase A. Indeed, RNase A treatment increased the total amount of immunoprecipitated DNA by 2- to 10-fold with respect to the untreated chromatin, with some variations between replicates and antibodies used (Figures 4B and S4B). We also confirmed that this increase in immunoprecipitated DNA does not occur when RNA is depleted from chromatin isolated from iPSCs under condition M (Figure S4C). These results strongly indicate that RNase treatment under condition L does not lead to the depletion of PRC2-bound chromatin but, in fact, leads to a gain of non-targeted chromatin.

Loss of ChIP signals after RNase treatment as a normalization artifact

The data thus far indicate that RNase A treatment leads to the depletion of ChIP signals for PRC2 subunits and H3K27me3 (Figures 2 and 3) but also to a global gain of non-targeted DNA (Figures 4A, 4B, S4A, and S4B). The simplest explanation for these observations is that the apparent depletion of rChIP-seq signals here (Figures 2 and 3) and elsewhere[26] resulted from a normalization artifact. Such an artifact could occur if DNA at target genes is normalized against DNA elsewhere. This is a common practice with ChIP-seq normalization, where signals are normalized against the total aligned reads. The artificial reduction of ChIP-seq signals after RNase A treatment is expected to persist under most types of commonly used normalization approaches. This is because the loss of ChIP-seq signal is, in fact, attributed to a gain in the background; DNA from non-targeted chromatin is sequenced at the expense of DNA from targeted chromatin. As a demonstration of this effect, when rChIP-qPCR signals from the repressed *HOXA10* gene are normalized against the active

GAPDH or *CCNA2* transcription start sites (TSS), both the SUZ12 and H3K27me3 enrichments appeared reduced after RNase A treatment (Figures 4C and S4D). Conversely, we did not observe an artificial reduction of H3K27me3 if the iPSC chromatin was treated under condition M (Figures S4E and S4F).

Collectively, our results indicate that the complete depletion of RNA from chromatin is insufficient to alter PRC2 chromatin occupancy (Figure 1; condition M in Table S1). Yet, rChIP conditions that lead to the apparent depletion of PRC2 from chromatin also lead to the depletion of H3K27me3 (Figures 2 and 3 and condition L in Table S1). All of these observations can be explained by a global gain of non-targeted DNA after RNase A treatment (Figures 4A–4C, S4A, and S4C), which artificially leads to the reduction of ChIP-seq signals as a result of a normalization artifact (Figures 4B–4D and S4B).

DISCUSSION

RNA has been shown to play an architectural role in chromatin organization and to be essential for the integrity of both constitutive and facultative heterochromatin.[2,6,8,9,11,25,28–30] While RNase treatment of chromatin has been central in these studies, we are only beginning to understand how this treatment affects the biophysical properties of chromatin. In practice, RNA degradation may reduce the solubility of chromatin under some ChIP conditions and buffers. Indeed, the observation that RNase treatment alters the structural properties of chromatin and leads to the formation of ''massive clumps'' has been reported at least since the 1980s.[6,28] Our analyses point to challenges in interpreting ChIP results if performed with RNase A treatment.

Our observations imply that a previous proposal of an ''RNA bridge'' between PRC2 and chromatin[26] has been supported based on an experimental artifact; RNase treatment under certain ChIP conditions (condition L; Figures 2 and 3; Long et al.[26]) leads to a gain of non-targeted DNA (Figures 4 and S4). We speculate that this could be the result of reduced chromatin solubility in the absence of RNA, which, in turn, leads to more chromatin precipitating with the beads (Figure 4D). In agreement with this, two independent parallel studies confirmed this phenomenon; Hickman and Jenner[43] demonstrated that precipitated chromatin could be visually detected on the beads after RNase A treatment, and Long et al.[42] quantified excess DNA in the IP sample after RNase A treatment.

RNase A treatment has been shown to increase the tendency of chromatin to precipitate, especially when carried out in the presence of a low concentration of monovalent salt.[44] This salt effect could be a potential explanation for why condition L leads to RNase A-dependent depletion of ChIP signals (Figures 2, 3, and 4;[26]) while condition M does not (Figure 1): condition L (Table S1; Long et al.[26]) contains less monovalent salt in the sonication buffer than condition M (Table S1). The salt effect could have been further amplified in the case of condition L, where whole-cell lysates were isolated as opposed to nuclear lysates under condition M (Table S1). Specifically, the lack of a nuclear isolation step under condition L could have increased the total amount of RNA during the sonication and IP with respect to condition M, which included nuclear isolation (Table S1). The excess RNA under condition L could have solubilized chromatin despite the low salt in the sonication buffer, possibly given its negative charge. Consistent with a potential role of RNA negative charges in solubilizing chromatin, a parallel study demonstrated that the anionic polymer poly-L-glutamic acid (PGA) is capable of restoring ChIP signals after RNase treatment.[43] In further support of this model, another parallel independent study demonstrated that the catalytic activity of RNase A is required for the depletion of ChIP-seq signals.[42] Hence, as soon as RNA is eliminated under condition L, the low salt may have caused chromatin to precipitate. Once non-targeted chromatin is precipitated with the beads, ChIP-seq signals are reduced because excess DNA from non-targeted chromatin is sequenced at the expense of DNA from targeted chromatin.

The original study[26] did not include H3K27me3 as a control for rChIP, while we did (Figures 1, 2, 3, and 4). Yet, they did use antibodies for the euchromatic factors RBP1 and TBP, which were not sensitive to RNase A digestion.[26] We were unable to reproduce these results; in our hands, RNase A treatment also led to the reduction of ChIP-seq signals and gain of DNA in the case of RBP1 (Figures 3 and 4). RNase A treatment increased the amount of DNA that precipitated with all antibodies tested, with some variations between different antibodies and independent replicates (Figure 4B). Variations in the amount of immunoprecipitated DNA were accompanied by variations in the rChIP-seq signals (compare Figures 2A, 2B, and S2A). These observations suggest suboptimal robustness of rChIP under condition L, in agreement with recent data from an independent study.[42] The global gain of DNA after ChIP with RNase treatment (Figures 4 and S4) does not fit well with the disruption of RNA bridges between the targeted factor and chromatin.

Our results do not reflect poorly on previous studies that used RNase treatment for applications other than ChIP. It is also important to note that our work cannot absolutely exclude the possibility of an RNA bridge between PRC2 and chromatin. Yet, our results firmly support two conclusions: (1) RNA is dispensable for the PRC2 chromatin occupancy after cells were already crosslinked and chromatin has been isolated (Figure 1), and (2) the ''RNA bridging'' model for PRC2 chromatin occupancy[26] has been supported based on an experimental artifact (Figure 4). RNase treatment will likely remain useful for the study of RNA-mediated regulation of chromatin modifiers as long as the global biophysical effects of RNA degradation are considered and controlled for.

Limitations of the study

Our study was designed to determine whether RNase A treatment under condition L reports real changes in PRC2 chromatin occupancy or, rather, whether it leads to the artificial depletion of ChIP-seq signals. Our study was not designed to identify the responsible determinant within condition L; yet, biochemical analysis by Dueva et al.[44] points to the concentration of monovalent salt as a key determinant of chromatin solubility after RNase A treatment. Accordingly, condition L is characterized by a low concentration of monovalent salt compared with condition M.

We did not characterize condition M as thoroughly as we characterized condition L. This is because our study was not designed to exclude an RNA bridge between PRC2 and chromatin but, rather, to examine evidence used previously to support it.

Future studies would have to demonstrate the robustness of rChIP under condition M or other conditions if they are to be used for discovery research. Demonstration of rChIP robustness would be important, given the variations in the amount of the immunoprecipitated DNA on different days under condition L and while using different antibodies. The experiments here may serve to guide this process.

STAR★METHODS

Detailed methods are provided in the online version of this paper and include the following:

- KEY RESOURCES TABLE
- RESOURCE AVAILABILITY
  - Lead contact
  - Materials availability
  - Data and code availability
- EXPERIMENTAL MODEL AND SUBJECT PARTICIPANT DETAILS
- METHOD DETAILS
  - Formaldehyde crosslinking for chromatin immunoprecipitation (ChIP)
  - ChIP conditions resulting in no changes to the PRC2 occupancy following RNase A treatment (condition M)
  - ChIP conditions resulting in RNase-dependent loss of PRC2 occupancy (rChIP; condition L)
  - Antibodies
  - ChIP-qPCR primer sequences
  - ChIP-seq library preparation
- QUANTIFICATION AND STATISTICAL ANALYSIS
  - Bioinformatic analysis of ChIP-Seq (+/− RNase A) datasets

SUPPLEMENTAL INFORMATION

Supplemental information can be found online at https://doi.org/10.1016/j.celrep.2024.113858.

ACKNOWLEDGMENTS

We are grateful to the members of the Davidovich lab for helpful discussions in relation to this work. We thank Richard Jenner, Tom Cech, and John Rinn for discussions of our work. We would also like to thank the MASSIVE HPC facility for support. Q.Z. is supported by investigator grant EL1 (APP1196365) from the National Health and Medical Research Council (NHMRC). C.D. is an EMBL-Australia Group Leader and a Sylvia and Charles Viertel Senior Medical Research Fellow and acknowledges support from the NHMRC (GNT1184637, GNT2011767, and GNT2020900). This research was partially funded by the Victoria State Government through mRNA Victoria.

AUTHOR CONTRIBUTIONS

E.H., Q.Z., and C.D. conceived the project and designed the experiments. E.H. and Q.Z. carried out all lab-based experiments. E.H., Q.Z., and E.H.G. performed the bioinformatics analyses of ChIP-seq datasets. G.S., M.B., V.P., P.P.D., and J.M.P. provided expertise regarding the culturing of human and mouse pluripotent stem cells. S.C.A. cultured mESCs for the rChIP experiments in Figure 2. E.H. and C.D. co-wrote the manuscript. C.D. supervised.

DECLARATION OF INTERESTS

The authors declare no competing interests.

Received: October 27, 2023
Revised: December 8, 2023
Accepted: February 8, 2024
Published: February 27, 2024

REFERENCES

1. Djebali, S., Davis, C.A., Merkel, A., Dobin, A., Lassmann, T., Mortazavi, A., Tanzer, A., Lagarde, J., Lin, W., Schlesinger, F., et al. (2012). Landscape of transcription in human cells. Nature *489*, 101–108.
2. Creamer, K.M., Kolpa, H.J., and Lawrence, J.B. (2021). Nascent RNA scaffolds contribute to chromosome territory architecture and counter chromatin compaction. Mol. Cell *81*, 3509–3525.e5.
3. Quinodoz, S.A., Jachowicz, J.W., Bhat, P., Ollikainen, N., Banerjee, A.K., Goronzy, I.N., Blanco, M.R., Chovanec, P., Chow, A., Markaki, Y., et al. (2021). RNA promotes the formation of spatial compartments in the nucleus. Cell *184*, 5775–5790.e30.
4. Bell, J.C., Jukam, D., Teran, N.A., Risca, V.I., Smith, O.K., Johnson, W.L., Skotheim, J.M., Greenleaf, W.J., and Straight, A.F. (2018). Chromatin-associated RNA sequencing (ChAR-seq) maps genome-wide RNA-to-DNA contacts. Elife *7*, e27024.
5. Pandey, R.R., Mondal, T., Mohammad, F., Enroth, S., Redrup, L., Komorowski, J., Nagano, T., Mancini-Dinardo, D., and Kanduri, C. (2008). Kcnq1ot1 Antisense Noncoding RNA Mediates Lineage-Specific Transcriptional Silencing through Chromatin-Level Regulation. Mol. Cell *32*, 232–246.
6. Rodríguez-Campos, A., and Azorín, F. (2007). RNA Is an Integral Component of Chromatin that Contributes to Its Structural Organization. PLoS One *2*, e1182.
7. Bhat, P., Honson, D., and Guttman, M. (2021). Nuclear compartmentalization as a mechanism of quantitative control of gene expression. Nat. Rev. Mol. Cell Biol. *22*, 653–670.
8. Caudron-Herger, M., and Rippe, K. (2012). Nuclear architecture by RNA. Curr. Opin. Genet. Dev. *22*, 179–187.
9. Maison, C., Bailly, D., Peters, A.H.F.M., Quivy, J.P., Roche, D., Taddei, A., Lachner, M., Jenuwein, T., and Almouzni, G. (2002). Higher-order structure in pericentric heterochromatin involves a distinct pattern of histone modification and an RNA component. Nat. Genet. *30*, 329–334.
10. Caudron-Herger, M., Müller-Ott, K., Mallm, J.P., Marth, C., Schmidt, U., Fejes-Tóth, K., and Rippe, K. (2011). Coding RNAs with a non-coding function: Maintenance of open chromatin structure. Nucleus *2*, 410–424.
11. Thakur J. and Henikoff S. Architectural RNA is required for heterochromatin organization. Preprint at bioRxiv. doi: https://doi.org/10.1101/784835.
12. Statello, L., Guo, C.-J., Chen, L.-L., and Huarte, M. (2021). Gene regulation by long non-coding RNAs and its biological functions. Nat. Rev. Mol. Cell Biol. *22*, 96–118.
13. Deevy, O., and Bracken, A.P. (2019). PRC2 functions in development and congenital disorders. Dev. Camb. Engl. *146*, dev181354.
14. Parreno, V., Martinez, A.-M., and Cavalli, G. (2022). Mechanisms of Polycomb group protein function in cancer. Cell Res. *32*, 231–253.
15. Owen, B.M., and Davidovich, C. (2022). DNA binding by polycomb-group proteins: searching for the link to CpG islands. Nucleic Acids Res. *50*, 4813–4839.
16. Davidovich, C., Zheng, L., Goodrich, K.J., and Cech, T.R. (2013). Promiscuous RNA binding by Polycomb repressive complex 2. Nat. Struct. Mol. Biol. *20*, 1250–1257.
17. Wang, X., Goodrich, K.J., Gooding, A.R., Naeem, H., Archer, S., Paucek, R.D., Youmans, D.T., Cech, T.R., and Davidovich, C. (2017). Targeting of

Polycomb Repressive Complex 2 to RNA by Short Repeats of Consecutive Guanines. Mol. Cell *65*, 1056–1067.e5.

18. Beltran, M., Tavares, M., Justin, N., Khandelwal, G., Ambrose, J., Foster, B.M., Worlock, K.B., Tvardovskiy, A., Kunzelmann, S., Herrero, J., et al. (2019). G-tract RNA removes Polycomb repressive complex 2 from genes. Nat. Struct. Mol. Biol. *26*, 899–909.
19. Almeida, M., Bowness, J.S., and Brockdorff, N. (2020). The many faces of Polycomb regulation by RNA. Curr. Opin. Genet. Dev. *61*, 53–61.
20. Davidovich, C., and Cech, T.R. (2015). The recruitment of chromatin modifiers by long noncoding RNAs: lessons from PRC2. RNA *21*, 2007–2022.
21. Healy, E., Mucha, M., Glancy, E., Fitzpatrick, D.J., Conway, E., Neikes, H.K., Monger, C., Van Mierlo, G., Baltissen, M.P., Koseki, Y., et al. (2019). PRC2.1 and PRC2.2 Synergize to Coordinate H3K27 Trimethylation. Mol. Cell *76*, 437–452.e6.
22. Glancy, E., Wang, C., Tuck, E., Healy, E., Amato, S., Neikes, H.K., Mariani, A., Mucha, M., Vermeulen, M., Pasini, D., and Bracken, A.P. (2023). PRC2.1- and PRC2.2-specific accessory proteins drive recruitment of different forms of canonical PRC1. Mol. Cell *83*, 1393–1411.e7.
23. Højfeldt, J.W., Laugesen, A., Willumsen, B.M., Damhofer, H., Hedehus, L., Tvardovskiy, A., Mohammad, F., Jensen, O.N., and Helin, K. (2018). Accurate H3K27 methylation can be established de novo by SUZ12-directed PRC2. Nat. Struct. Mol. Biol. *25*, 225–232.
24. Højfeldt, J.W., Hedehus, L., Laugesen, A., Tatar, T., Wiehle, L., and Helin, K. (2019). Non-core Subunits of the PRC2 Complex Are Collectively Required for Its Target-Site Specificity. Mol. Cell *76*, 423–436.e3.
25. Beltran, M., Yates, C.M., Skalska, L., Dawson, M., Reis, F.P., Viiri, K., Fisher, C.L., Sibley, C.R., Foster, B.M., Bartke, T., et al. (2016). The interaction of PRC2 with RNA or chromatin is mutually antagonistic. Genome Res. *26*, 896–907.
26. Long, Y., Hwang, T., Gooding, A.R., Goodrich, K.J., Rinn, J.L., and Cech, T.R. (2020). RNA is essential for PRC2 chromatin occupancy and function in human pluripotent stem cells. Nat. Genet. *52*, 931–938.
27. Zhang, Q., McKenzie, N.J., Warneford-Thomson, R., Gail, E.H., Flanigan, S.F., Owen, B.M., Lauman, R., Levina, V., Garcia, B.A., Schittenhelm, R.B., et al. (2019). RNA exploits an exposed regulatory site to inhibit the enzymatic activity of PRC2. Nat. Struct. Mol. Biol. *26*, 237–247.
28. Nickerson, J.A., Krochmalnic, G., Wan, K.M., and Penman, S. (1989). Chromatin architecture and nuclear RNA. Proc. Natl. Acad. Sci. *86*, 177–181.
29. Derenzini, M., Pession-Brizzi, A., and Novello, F. (1981). Relationship between ribonucleoprotein particle, containing heterogeneous RNA and ultrastructure and function of chromatin in purified rat hepatocyte nuclei. J. Ultrastruct. Res. *77*, 66–82.
30. Wong, L.H., Brettingham-Moore, K.H., Chan, L., Quach, J.M., Anderson, M.A., Northrop, E.L., Hannan, R., Saffery, R., Shaw, M.L., Williams, E., and Choo, K.H.A. (2007). Centromere RNA is a key component for the assembly of nucleoproteins at the nucleolus and centromere. Genome Res. *17*, 1146–1160.
31. Bernstein, E., Duncan, E.M., Masui, O., Gil, J., Heard, E., and Allis, C.D. (2006). Mouse polycomb proteins bind differentially to methylated histone H3 and RNA and are enriched in facultative heterochromatin. Mol. Cell Biol. *26*, 2560–2569.
32. Casale, A.M., Cappucci, U., Fanti, L., and Piacentini, L. (2019). Heterochromatin protein 1 (HP1) is intrinsically required for post-transcriptional regulation of Drosophila Germline Stem Cell (GSC) maintenance. Sci. Rep. *9*, 4372.
33. Thompson, P.J., Dulberg, V., Moon, K.M., Foster, L.J., Chen, C., Karimi, M.M., and Lorincz, M.C. (2015). hnRNP K Coordinates Transcriptional Silencing by SETDB1 in Embryonic Stem Cells. PLoS Genet. *11*, e1004933.
34. Abruzzi, K.C., Lacadie, S., and Rosbash, M. (2004). Biochemical analysis of TREX complex recruitment to intronless and intron-containing yeast genes. EMBO J. *23*, 2620–2631.
35. Bernard, P., Drogat, J., Dheur, S., Genier, S., and Javerzat, J.-P. (2010). Splicing Factor Spf30 Assists Exosome-Mediated Gene Silencing in Fission Yeast. Mol. Cell Biol. *30*, 1145–1157.
36. Frank, S.R., Schroeder, M., Fernandez, P., Taubert, S., and Amati, B. (2001). Binding of c-Myc to chromatin mediates mitogen-induced acetylation of histone H4 and gene activation. Genes Dev. *15*, 2069–2082.
37. Bracken, A.P., Kleine-Kohlbrecher, D., Dietrich, N., Pasini, D., Gargiulo, G., Beekman, C., Theilgaard-Mönch, K., Minucci, S., Porse, B.T., Marine, J.C., et al. (2007). The Polycomb group proteins bind throughout the INK4A-ARF locus and are disassociated in senescent cells. Genes Dev. *21*, 525–530.
38. Conway, E., Jerman, E., Healy, E., Ito, S., Holoch, D., Oliviero, G., Deevy, O., Glancy, E., Fitzpatrick, D.J., Mucha, M., et al. (2018). A Family of Vertebrate-Specific Polycombs Encoded by the LCOR/LCORL Genes Balance PRC2 Subtype Activities. Mol. Cell *70*, 408–421.e8.
39. Pasini, D., Bracken, A.P., Hansen, J.B., Capillo, M., and Helin, K. (2007). The Polycomb Group Protein Suz12 Is Required for Embryonic Stem Cell Differentiation. Mol. Cell Biol. *27*, 3769–3779.
40. Bracken, A.P., Pasini, D., Capra, M., Prosperini, E., Colli, E., and Helin, K. (2003). EZH2 is downstream of the pRB-E2F pathway, essential for proliferation and amplified in cancer. EMBO J. *22*, 5323–5335.
41. Bracken, A.P., Dietrich, N., Pasini, D., Hansen, K.H., and Helin, K. (2006). Genome-wide mapping of Polycomb target genes unravels their roles in cell fate transitions. Genes Dev. *20*, 1123–1136.
42. Long, Y., Hwang, T., Gooding, A.R., Goodrich, K.J., Vallery, T.K., Rinn, J.L., and Cech, T.R. (2023). Evaluation of the RNA-dependence of PRC2 binding to chromatin in human pluripotent stem cells. Preprint at bioRxiv. https://doi.org/10.1101/2023.08.17.553776.
43. Hickman A.H. & Jenner R. G. Apparent RNA bridging between PRC2 and chromatin is an artefact of nonspecific chromatin precipitation upon RNA degradation. Preprint at bioRxiv. doi: https://doi.org/10.1101/2023.08.16.553503.
44. Dueva, R., Akopyan, K., Pederiva, C., Trevisan, D., Dhanjal, S., Lindqvist, A., and Farnebo, M. (2019). Neutralization of the Positive Charges on Histone Tails by RNA Promotes an Open Chromatin Structure. Cell Chem. Biol. *26*, 1436–1449.e5.
45. Liu, X., Nefzger, C.M., Rossello, F.J., Chen, J., Knaupp, A.S., Firas, J., Ford, E., Pflueger, J., Paynter, J.M., Chy, H.S., et al. (2017). Comprehensive characterization of distinct states of human naive pluripotency generated by reprogramming. Nat. Methods *14*, 1055–1062.
46. Langmead, B., and Salzberg, S.L. (2012). Fast gapped-read alignment with Bowtie 2. Nat. Methods *9*, 357–359.
47. Li, H., Handsaker, B., Wysoker, A., Fennell, T., Ruan, J., Homer, N., Marth, G., Abecasis, G., and Durbin, R.; 1000 Genome Project Data Processing Subgroup (2009). The Sequence Alignment/Map format and SAMtools. Bioinformatics *25*, 2078–2079.
48. Zhang, Y., Liu, T., Meyer, C.A., Eeckhoute, J., Johnson, D.S., Bernstein, B.E., Nusbaum, C., Myers, R.M., Brown, M., Li, W., and Liu, X.S. (2008). Model-based Analysis of ChIP-Seq (MACS). Genome Biol. *9*, R137.
49. Ramírez, F., Ryan, D.P., Grüning, B., Bhardwaj, V., Kilpert, F., Richter, A.S., Heyne, S., Dündar, F., and Manke, T. (2016). deepTools2: a next generation web server for deep-sequencing data analysis. Nucleic Acids Res. *44*, W160–W165.

STAR★METHODS

KEY RESOURCES TABLE

REAGENT or RESOURCE	SOURCE	IDENTIFIER
Antibodies		
Anti-EZH2 rabbit monoclonal	Cell Signaling	Cat #5246; RRID:AB_10694683
Anti-SUZ12 rabbit monoclonal	Cell Signaling	Cat #3737; RRID:AB_2196850
Anti-H3K27me3 rabbit monoclonal (custom formulation; BSA & Azide free)	Cell Signaling	Cat #9733 (C36B11); RRID:AB_2616029
Anti-H3K27Ac rabbit polyclonal	Abcam	Cat #ab4729; RRID:AB_2118291
Anti-RPB1 rabbit monoclonal	Cell Signaling	Cat #14958; RRID:AB_2687876
Chemicals, peptides, and recombinant proteins		
RNase A, DNase and protease-free (10 mg/mL)	Thermo Fisher Scientific	Cat# EN0531
Leukemia Inhibitory Factor (LIF)	Millipore	Cat# ESG1107
Proteinase K	Thermo Fisher Scientific	Cat# EO0491
Protein G Dynabeads	Thermo Fisher Scientific	Cat# 10004D
TRIzol Reagent	Thermo Fisher Scientific	Cat# 15596018
RNase-Free DNase Set	Qiagen	Cat# 79254
Protease Inhibitor Cocktail	Merck (Sigma-Aldrich)	Cat# P8340
NEBNext Sample Purification Beads	New England Biolabs	Cat# E7767S
QuantiNova SYBR Green PCR kit	Qiagen	Cat# 208054
Critical commercial assays		
QIAquick PCR purification kit	Qiagen	Cat# 28106
RNeasy MinElute Cleanup Kit	Qiagen	Cat# 4204
Agilent D1000 High Sensitivity DNA kit	Agilent	Cat# 5067-5584
NEBNext Ultra II DNA Library Prep Kit for Illumina	New England Biolobs	Cat# E7645
Qubit dsDNA High Sensitivity Assay Kit	Thermo Fisher Scientific	Cat# Q32854
NEBNext Multiplex Oligos for Illumina (Seq #1 & #2)	New England Biolobs	Cat# E7335; E7500
Deposited data		
Next-generation sequencing files	This study	GEO: GSE240079
Raw imaging data	This study	Mendeley data: https://data.mendeley.com/datasets/c2j6dgw8xt/2
Experimental models: Cell lines		
Mouse: ES cell line	Monash Genome Modification Platform	Strain: Bruce4-CS
Human: iPS cell line	Jose Polo Lab	Liu et al.[45]
K562 cell line	Davidovich Lab	ATCC
Oligonucleotides		
See Table S2.	This paper	N/A
Software and algorithms		
Bowtie2 v2.3.5	Langmead & Salzberg[46]	https://bowtie-bio.sourceforge.net/bowtie2/index.shtml
SAMtools v1.9-gcc5	Li et al.[47]	https://www.htslib.org/doc/samtools.html
MACS2 v2.1.1	Zhang et al.[48]	https://github.com/macs3-project/MACS
deepTools2 v3.1.3	Ramirez et al.[49]	https://deeptools.readthedocs.io/en/develop/index.html

RESOURCE AVAILABILITY

Lead contact

Further information and requests for resources should be directed to and will be fulfilled by the lead contact, Chen Davidovich (chen.davidovich@monash.edu).

Materials availability

All cell lines used in this study are available upon request from the lead contact.

Data and code availability

- All next-generation sequencing datasets have been deposited in the GEO repository with code GSE240079 and raw imaging data was deposited to Mendeley Data (https://data.mendeley.com/datasets/c2j6dgw8xt/1) and will be publicly available from the date of publication. Accession numbers are also listed in the Key resources table.
- This paper does not report original code.
- Any additional information required to reanalyse the data reported is available upon request from the lead contact.

EXPERIMENTAL MODEL AND SUBJECT PARTICIPANT DETAILS

Mouse embryonic stem cells (mESCs) were grown on gelatinised culture dishes (0.1%) in DMEM supplemented with 10% FBS (Scientifix; FBSAU-2007A), 1% (v/v) penicillin-streptomycin (Thermo Scientific #15140122), 50 μM beta-mercaptoethanol (Millipore; ES-007-E), 1:100 non-essential amino acids, 1:100 sodium pyruvate, 1:100 GlutaMax (all GIBCO) and ESGRO leukemia inhibitory factor (LIF) (Millipore; ESG1107; 10,000x).

K562 cells were cultured in RPMI-1640 (Merck #R8758) growth medium supplemented with 10% FBS (Cellsera AU-FBS/SF) and 1% (v/v) penicillin-streptomycin (Thermo Scientific #15140122) and were incubated at 37°C with 5% CO_2. K562 cells were acquired from ATCC.

Human induced pluripotent stem cells (iPS) were derived from HDFn (neonatal human dermal fibroblasts) according to.[45] HDFn iPS cells were maintained in a feeder-free system on vitronectin (VTN-N; Gibco; A31804) coated tissue culture plastics in Essential 8 Flex medium (Gibco; A2858501). Cells were incubated at 37°C and 5% CO_2 and passaged every 2–3 days using 0.5 mM EDTA. Human iPS cells were obtained from the Jose Polo Lab. All cell lines were tested periodically for mycoplasma contamination.

METHOD DETAILS

Formaldehyde crosslinking for chromatin immunoprecipitation (ChIP)

Mouse ESC, K562 or human iPS cells were collected, counted, and washed once with PBS before crosslinking for 10 min with PBS containing 1% formaldehyde (Sigma). Cells were crosslinked in 15 mL falcon tubes at a density of ~5 × 10^6 cells/mL. Crosslinking was quenched with 0.125 M Glycine prior to two PBS washes. Crosslinked cells were then snap-frozen on liquid nitrogen and stored at −80°C before proceeding with the rest of the ChIP assay.

ChIP conditions resulting in no changes to the PRC2 occupancy following RNase A treatment (condition M)

ChIP assay was performed as described previously.[21,36,39,40] See Table S1 for more details. Crosslinked cells were thawed on ice and lysed in 5 mL of SDS-Lysis buffer (100 mM NaCl, 50 mM Tris pH 8.1, 5 mM EDTA pH 8.0, 0.5% SDS, 1X protease inhibitor cocktail [Sigma; P8340]). Nuclei and chromatin were pelleted by centrifugation at 1200 rpm for 6 min at room temperature. The supernatant was then discarded, and the pellet was resuspended in 2 mL of ChIP buffer (33 mM Tris-HCl pH 8, 100 mM NaCl, 5 mM EDTA, 0.33% SDS, 1.67% Triton X-100, 1X protease inhibitor cocktail [Sigma; P8340]). Chromatin was sheared to approximately 200 bp to 500 bp fragments by sonication using a Bioruptor Plus (Diagenode) at high power. Total sonication time (i.e., cumulative "on" time) was 15min with 30 s on/off pulses. Sonicated chromatin was incubated overnight with antibody while rotating at 4°C. Prior to overnight incubation with antibodies, an input sample was taken (1%). RNase A (DNase and protease-free Thermo Fisher Scientific; #EN0531) was added along with the antibody to the plus RNase A samples at a final concentration of 5–50 μg/mL. Extract from 2.5 × 10^6 cells were used per ChIP (+/− RNase A). The following morning, samples were clarified by centrifugation at 20,000 g for 20 min at 4°C. Following clarification, the chromatin was incubated for 3 h with Protein G Dynabeads (ThermoFisher; 10004D; 50 μL beads were used per ChIP). After incubation, the beads were washed three times in Mixed Micelle Buffer (150 mM NaCl, 20 mM Tris pH 8.1, 5 mM EDTA pH 8.0, 5.2% Sucrose, 1% Triton X-100, 0.2% SDS), twice with Buffer 500 (0.1% Sodium Deoxycholate, 1 mM EDTA pH 8.0, 50 mM HEPES pH 7.5, 1% Triton X-100), twice with LiCl detergent wash (0.5% Sodium Deoxycholate, 1 mM EDTA pH 8.0, 250 mM LiCl, 0.5% NP-40,10 mM Tris pH 8.0) and finally, one wash with TE. All the washes were performed at 4°C. Immunoprecipitated material was eluted from the beads with 100 μL elution buffer (0.1 M NaHCO3, 1% SDS) while shaking for 1 h at 65°C. The supernatant was retained and incubated overnight at 65°C while shaking to reverse the crosslinks. The eluted material was then subjected to RNase A (DNase and protease-free Thermo Fisher Scientific; #EN0531) and Proteinase K (ThermoFisher; #EO0491) treatments prior to DNA clean up (QIAGEN MinElute PCR Purification Kit Cat#28004). ChIP enrichments were analyzed by qPCR using the QuantiNova SYBR Green PCR kit (Qiagen; 208054).

When testing RNase A efficiency during the rChIP assay, 10% of lysate was removed following overnight immunoprecipitation and RNase A treatment. Protein was removed with Proteinase K (ThermoFisher; #EO0491) and crosslinks reversed for 2 hrs at 55°C. RNA was extracted with 1 mL TRIzol and 200 μL chloroform, inverted several times and centrifuged at 20,000g for 20 min at 4°C. The aqueous layer was then passed through a QIAGEN RNeasy minElute column. Following one wash with RWT buffer DNA was digested on the column with DNase I for 15 min at room temperature. Following washes in RPE buffer RNA was eluted in RNase free water and analyzed by electrophoresis on an agarose gel and quantified using the Qubit RNA High Sensitivity Assay Kit (ThermoFisher Q32852).

ChIP conditions resulting in RNase-dependent loss of PRC2 occupancy (rChIP; condition L)

ChIP assay with RNase A treatment was performed based on a previous study.[26] See Table S1 for more details. Specifically, cross-linked cells were thawed on ice, lysed in 2 mL lysis buffer (50 mM Tris-Cl pH 8.1, 10 mM EDTA, 0.5–1.0% SDS, plus 1X protease inhibitor cocktail [Sigma; P8340]) and incubated on ice for 10 min. Chromatin was sheared to approximately 200bp-500bp fragments by sonication using a Bioruptor Plus (Diagenode) at high power. Total sonication time (e.g., total "on" time) was 20 min with 30 s on/off pulses. After sonication, the lysate was cleared by centrifugation at 16,300 g for 10 min at 4°C. The supernatant was stored at −80°C or used directly in the ChIP assay. Lysate was diluted 1:5 in IP buffer (16.7 mM Tris-HCl pH 8.1, 1.2 mM EDTA, 167 mM NaCl, 1% Triton X-100 and 1X protease inhibitor cocktail [Sigma; P8340]) and pre-cleared with 50 μL protein G Dynabeads (ThermoFisher; 10004D) for 1 h at 4°C. The sonicated lysate was incubated overnight with antibody while rotating at 4°C. Prior to overnight incubation with the antibodies, an input sample was taken (1%). RNase A (DNase and protease-free Thermo Fisher Scientific; #EN0531) was added along with the antibody to the plus RNase A samples at a final concentration of 50 μg/mL. Extracts from 2.5 × 10^6 cells were used per ChIP (+/− RNase A). The Next morning, Protein G Dynabeads were equilibrated in IP buffer: 25 μL beads were added to each ChIP and incubated for 1 h at 4°C. After incubation, beads were washed twice in low salt buffer (20 mM Tris-HCl pH 8.0, 2 mM EDTA, 150 mM NaCl, 0.1% SDS, 1% Triton X-100), twice with high salt buffer (20 mM Tris-HCl pH 8.0, 2 mM EDTA, 500 mM NaCl, 0.1% SDS, 1% Triton X-100), twice in LiCl buffer (10 mM Tris-HCl pH 8.0, 1 mM EDTA, 250 mM LiCl, 1% Sodium Deoxycholate (w/v), 1% NP-40 substitute) followed by one final wash in TE buffer (10 mM Tris pH 8.0, 1 mM EDTA). All the washes were performed at 4°C. Immunoprecipitated material was eluted from the beads with 120 μL elution buffer (0.1 M NaHCO3, 1% SDS) for 20 min at room temperature. The supernatant was retained and 200 mM NaCl was added and incubated along with input samples overnight at 65°C while shaking to reverse the crosslinks. The eluted material was then subjected to RNase A (DNase and protease-free Thermo Fisher Scientific; #EN0531) and Proteinase K (ThermoFisher; #EO0491) treatments prior to DNA clean up (QIAGEN MinElute PCR Purification Kit Cat#28004). ChIP enrichments were analyzed by qPCR using the QuantiNova SYBR Green PCR kit (Qiagen; 208054).

Antibodies

Anti-EZH2 (Cell Signaling; #5246), 8 μg per ChIP. Anti-SUZ12 (Cell Signaling; #3737), 0.3 μg per ChIP. Anti-H3K27me3 (Cell Signaling; C36B11), 5 μg per ChIP. Anti-H3K27Ac (Abcam; ab4729), 5 μg per ChIP. Anti-RPB1 (NTD) (Cell Signaling; #14958), 1 μg per ChIP.

ChIP-qPCR primer sequences

See Table S2.

ChIP-seq library preparation

Following ChIP (+/− RNase A) experiments, the precipitated DNA was quantified using the Qubit dsDNA High Sensitivity Assay Kit (ThermoFisher Q32854). A total of 1–10 ng of DNA from each ChIP experiment was used for library preparation using the NEBNext Ultra II DNA Library Kit for Illumina (E7645) and NEBNext Multiplex Oligos for Illumina (Set#1 & #2; E7335 & E7500). Following adaptor ligation, DNA was PCR amplified for 4–10 cycles, depending on the amount of the input DNA. DNA purification was then performed using NEBNext Sample Purification Beads (E7767S). The quality and size distributions of DNA libraries were ascertained on a TapeStation (Agilent) using High Sensitivity D1000 ScreenTape assay reagents (Agilent; 5067–5585). The resulting libraries were then used for cluster generation and sequencing on an Illumina-based platform with a 150 bp paired-end read format (2-3x10^7 reads per sample) (GeneWiz/Azenta).

QUANTIFICATION AND STATISTICAL ANALYSIS

Bioinformatic analysis of ChIP-Seq (+/− RNase A) datasets

Paired-end ChIP-Seq reads were aligned to a reference genome (mm10 or hg38) using Bowtie2 with default parameters.[46] SAMtools was used to convert SAM files to BAM files and to remove duplicate aligned reads.[47] Bigwig files were generated using bamCoverge from the deepTools suite (version 3.1.3)[49] with a bin size of 10 and scaled using CPM (counts per million) normalisation. All transcription start sites (TSS) for the mm10 (n = 19,888) and hg38 (n = 17,139) builds of the mouse and human genomes were defined and annotated as unique protein-coding TSS +/−5kb (downloaded from ENSEMBL biomart). Heatmaps were generated with these TSS annotation files using the computeMatrix and plotHeatmap tools from the deepTools suite.[49] Peak calling was performed using MACS2 v2.1.1[48] with parameters -format BAMPE and a p value cut-off of 1 × 10^{-4}.